

Physics-dynamics coupling with element-based high-order Galerkin methods: quasi equal-area physics grid

ADAM R. HERRINGTON*

School of Marine and Atmospheric Sciences, Stony Brook University, State University of New York, Stony Brook, New York.

PETER H. LAURITZEN

Climate and Global Dynamics, National Center for Atmospheric Research, 1850 Table Mesa Drive, Boulder, Colorado, USA.

MARK A. TAYLOR

Sandia National Laboratories, Albuquerque, New Mexico, USA.

STEVE GOLDHABER

Climate and Global Dynamics, National Center for Atmospheric Research, 1850 Table Mesa Drive, Boulder, Colorado, USA.

KEVIN A. REED

School of Marine and Atmospheric Sciences, Stony Brook University, State University of New York, Stony Brook, New York.

ABSTRACT

Enter the text of your abstract here.

1. Introduction

An increasing number of numerical methods publications in the atmospheric science literature concern transport, shallow-water, and three-dimensional models employing element-based high-order Galerkin discretizations such as finite-element and discontinuous Galerkin methods (for an introduction to these methods see, e.g., Durran 2010; Nair et al. 2011). Some global models based on Galerkin methods have reached a level of maturity for which they are being considered for next generation climate and weather models due to their inherent conservation properties, high-order accuracy (for smooth problems), high parallel efficiency, high processor efficiency, and geometric flexibility facilitating mesh-refinement applications. NCAR’s Community Atmosphere Model (CAM; Neale et al. 2010) offers a dynamical core based on continuous Galerkin finite elements (Taylor and Fournier 2010), referred to as CAM-SE (CAM

Spectral Elements; Dennis et al. 2012; Taylor et al. 2008; Lauritzen et al. 2017). CAM-SE is, in particular, being used for high resolution climate modeling (e.g., Small et al. 2014; Bacmeister et al. 2013; Reed et al. 2015) and static mesh-refinement applications (e.g., Fournier et al. 2004; Zarzycki et al. 2014a,b; Guba et al. 2014; Rhoades et al. 2016). Other examples of models based on high-order Galerkin methods that are being considered for ‘operational’ weather-climate applications are Giraldo and Restelli (2008), Nair et al. (2009) and Brdar et al. (2013).

Assumptions inherent to the physical parameterizations (also referred to as *physics*) require the state passed by the dynamical core to represent a ‘large-scale state’, for example, in quasi-equilibrium-type convection schemes (Arakawa and Schubert 1974; Plant 2008). In finite-volume methods, one may think of the dynamical core state as the average state of the atmosphere over a control volume, and for resolutions typical of climate simulations is entirely consistent with the notion of a ‘large-scale state’. For finite-difference methods the point value is thought of as representative for the atmospheric state in the vicinity of the point value and one can usually associate a volume with the grid-point. Hence the physics grid (the grid on

*Corresponding author address: Peter H. Lauritzen, Climate and Global Dynamics, National Center for Atmospheric Research, 1850 Table Mesa Drive, Boulder, Colorado, USA.
E-mail: pel@ucar.edu

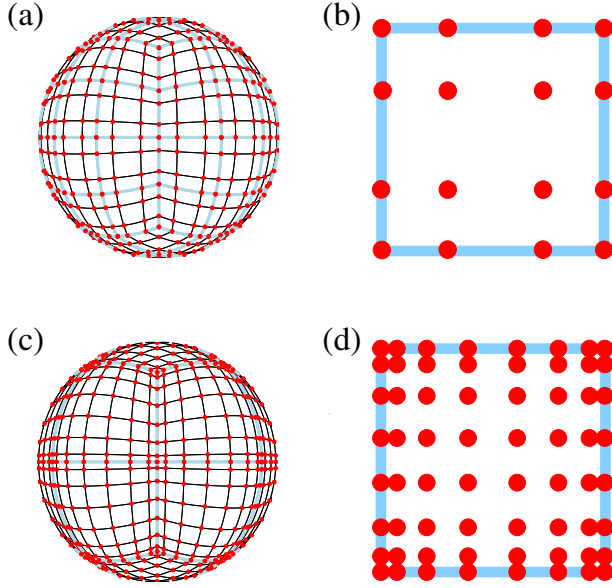


FIG. 1. Example of CAM-SE GLL quadrature grids, marked with red filled circles, (a & c) on the cubed-sphere and (b & d) in an element. (a)-(b) and (c)-(d) use 4×4 ($np = 4$) and 8×8 ($np = 8$) GLL quadrature points in each element, respectively. (a) and (c) have the same average grid-spacing at the Equator (7.5°) which is obtained by using (a) 4×4 ($ne = 4$) and (b) 2×2 ($ne = 2$) elements on each cubed-sphere face/panel, respectively. The element boundaries are marked with thick light blue lines. The grid configurations shown on (a) and (c) are referred to as $ne4np4$ and $ne2np8$, respectively.

which the state of the atmosphere is evaluated and passed to physics) and the dynamics grid (the grid the dynamical core uses) coincide. Having the physics and dynamics grids coincide is obviously convenient since no interpolation is needed (which could disrupt conservation properties) and the number of degrees of freedom on both grids is exactly the same.

For the regular latitude-longitude, cubed-sphere and icosahedral grids the distance between the grid-points is gradually varying for finite-volume/finite-difference discretizations. For high-order element-based Galerkin methods, the dynamical core grid is defined by the quadrature points. For the case of CAM-SE these are the Gauss-Lobatto-Legendre (GLL) quadrature points. A unique aspect of the high-order quadrature rules is that the nodes within an element are not equally spaced. For example, Figure 1 shows GLL points on an individual element of a cubed-sphere grid for degree 3 ($np = 4$ quadrature points) and degree 7 ($np = 8$ quadrature points) polynomial basis in CAM-SE. Both grids have the same average resolution on the sphere (due to different number of elements), however, the higher the order of the quadrature rule the less equi-distant are the quadrature points. GLL quadrature

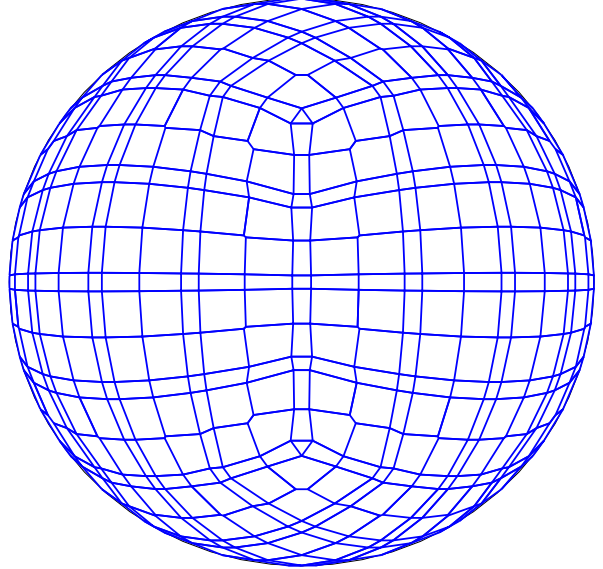


FIG. 2. An example of control volumes constructed around GLL quadrature points (NE4NP4) so that the spherical area of the control volumes exactly match the quadrature weight multiplied by the metric factor.

points cluster near the edges and, in particular, the corners of the elements.

If the conventional physics-dynamics coupling paradigm is applied to CAM-SE, then the physics are evaluated at the GLL nodes, and a volume associated with the quadrature point should be defined. An example of that is shown on Figure 2 where control volumes have been defined around the quadrature points so that the spherical area of the control volumes exactly match the Gaussian weight multiplied by the metric term (these weights are used for integrating the basis functions over the elements and can therefore, in this context, be interpreted as areas). [Mark: could we be mathematically more rigorous? perhaps an appendix describing the iterative algorithm?] This grid is used in the NCAR CESM (Community Earth System Model) coupler for passing states between ocean, atmosphere and land components since the current remapping method is finite-volume based and therefore requires control volumes¹. Hence the components ‘see’ an irregular atmospheric grid. Similarly, the parameterizations in the atmosphere ‘see’ a state that is anisotropically sampled in space (see Figure 1 and 5 in Kim et al. 2008).

It would be incorrect to interpret the irregular size of control volumes in Figure 2 as an equivalent spread in the scales of motion resolved by the dynamical core. The scales of motion are defined by the degree of the Lagrange

¹it is noted that methods exist that do not require control volumes for conservative interpolation (Ullrich and Taylor 2015)

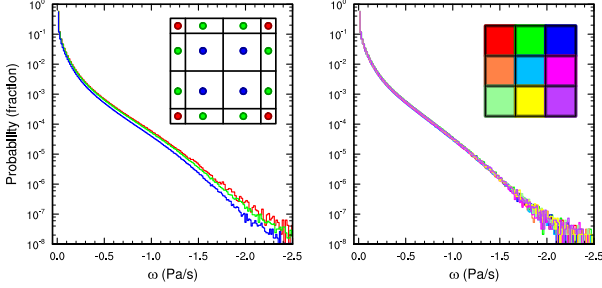


FIG. 3. Probability density distribution of instantaneous upward ω in a pair of aqua-planet simulations using CAM4 physics. Figure is constructed from one year of six hourly data, at all vertical levels. (Left) $ne30np4$ configuration conditionally sampled for interior, edge and corner node control volumes, and (Right) $ne30pg3$ configuration, but sampled by within-element physics grid-cell location. Note the consistently larger magnitude ω for boundary nodes compared with interior nodes, and that the bias is eliminated through mapping to a quasi-equal area physics grid.

basis in each element, and the nodes may be viewed as irregularly spaced samples of an underlying spectrally truncated state. From this perspective, one would expect the solution to be independent of control volume size. An aqua-planet simulation (Neale and Hoskins 2000; Medeiros et al. 2016) is carried out using CAM-SE (Figure 3), and the probability density distribution of the upward vertical pressure velocity (ω), conditionally sampled based on three categories - ‘interior nodes’, with their large grid cell areas, and ‘edge’ and ‘corner’ nodes with their characteristically smaller grid cell areas - is shown in Figure 3. There is an apparent dependence on control volume size, with interior nodes being characteristically sluggish and initially at odds with our expectation. However, the lack of a distinction between ‘corner’ and ‘edge’ solutions is inconsistent with our expectation. It turns out, that ‘corner’ and ‘edge’ solutions are similar because they have something else in common - they both lie on an element boundary. The division of solutions shown in Figure 3 is primarily between whether a node is, or is not situated on an element boundary, and is a nuanced signature of high-order element-based Galerkin methods for non-smooth problems.

The quadrature grid in element-based Galerkin methods is defined to perform mathematical operations on the basis functions, e.g., computing gradients and integrals, rather than evaluating the state variables for physics-dynamics coupling. While the interior quadrature nodes are high-order C^∞ in CAM-SE, the smoothness of boundary nodes are constrained by the need to patch neighboring solutions together to form a globally continuous solution, known as the direct stiffness summation (DSS). The DSS operation is attractive because it allows for high-order accuracy with minimal communication between elements, but re-

sults in a C^0 degradation at element boundaries (Figure 4). Through evaluating the physics at the nodal points, strong grid-scale forcing or oscillatory behavior near an element boundary may exacerbate the discontinuity (Figure 4). The greater magnitude vertical motion of boundary nodes in Figure 3 is therefore due to the systematically tighter pressure gradients on element boundaries. One may argue that it would be more consistent to integrate the basis functions over quasi-equal area control volumes within each element and pass those control volume average values to physics rather than irregularly spaced quadrature point values. In this case when integrating basis functions over control volumes a grid-cell average value is more representative of the values near the extrema at the element boundary than the quadrature point value. The relationship between the nodal values, the basis functions and the proposed control volumes is illustrated schematically in one-dimension in Figure 5.

It is the purpose of this paper to document the design of CAM-SE with an approximately isotropic physics grid, in which the physics and dynamics grids are entirely separated as illustrated in one dimension in Figure 5. The mapping procedures used in the physics grid configuration are presented in Section 2. Idealized model configurations with and without topography are presented in Section 3, illustrating a marked reduction in grid imprinting due to the use of a quasi-equal area physics grid. Section 4 contains a discussion of results and concluding remarks.

2. Methods

Here we focus on CAM-SE, however, in principle the methods apply to any element-based high-order Galerkin model. The physics grid in CAM-SE is defined by subdividing each element using equi-angular gnomonic coordinate lines to define the sides of the physics grid control volumes. Note that the element boundaries are defined by equi-angular gnomonic grid lines. The notation $pg = 3$ refers to the configuration where the elements are divided into $pg \times pg = 3 \times 3$ quasi equal-area physics grid cells (see Figure 6). Defining the physics grid by sub-dividing elements makes it possible to use the same infrastructure as used for the quadrature point values thereby facilitating its implementation in CAM-SE. Here we make use of the $ne30np4$ and $ne30pg3$ grids that use GLL quadrature point physics grid (physics and dynamics grid coincide), and the same ($pg = 3$) resolution quasi equal-area physics grids, respectively. In all configurations we use degree 3 Lagrange basis ($np = 4$) and $ne \times ne = 30 \times 30$ elements on each cubed-sphere panel resulting in an average GLL quadrature point spacing at the Equator of 1° . Vertical grid spacing is the standard CAM5 configuration ($nlev = 30$).

A consequence of separating physics and dynamics grids is that the atmospheric state must be mapped to the physics grid and the physics tendencies must be mapped

back to the dynamics grid. The dynamics state is defined on the GLL grid in terms of temperature $T^{(gll)}$, zonal wind component $u^{(gll)}$, meridional wind component $v^{(gll)}$, dry pressure level thickness $\Delta p^{(gll)}$ and dry tracer mixing ratio $m^{(gll)}$ (the procedure for mapping tracers is the same for all tracers so just one generic tracer is included in the notation/algorithim).

In the mapping of the atmospheric state to the physics grid it is important that the following properties are met:

1. conservation of scalar quantities such as mass and thermal energy,
2. for tracers; shape-preservation (monotonicity), i.e. the mapping method must not introduce new extrema in the interpolated field, in particular, negatives,
3. consistency, i.e. the mapping preserves a constant.

Other properties that may be important, but not pursued here, is total energy conservation and axial angular momentum conservation.

The physics tendencies are computed on the finite-volume physics grid and are denoted $f_T^{(phys)}$, $f_u^{(phys)}$, $f_v^{(phys)}$, and $f_m^{(phys)}$. Note that dry air mass is not modified by physics and hence there is no tendency for dry mass, $f_{\Delta p} \equiv 0$.

and must be mapped back to the GLL grid. It is important that this process:

1. preserves a zero tendency,
2. consistent, i.e. a constant tendency is constant on both grids.

It is argued that the most accurate and consistent method to transfer the dynamics state from the GLL grid to the physics grid is to integrate the SE basis function representation (Lagrange polynomials) over the physics grid control volumes. This satisfies property 1 and 3 but not necessarily 2 as the basis functions themselves are oscillatory. We will return to this issue.

Note that tendencies and not an updated state is mapped back to the dynamics grid. If one were to map an updated state the errors in the mapping process may adversely affect the simulation, e.g., in the case of no physics forcing there will be a non-zero ‘physics forcing’ entirely due to the errors in the mapping algorithm.

3. Results

The CAM aqua-planet reference configuration (Neale and Hoskins 2000; Medeiros et al. 2016) consists of an ocean covered planet in a perpetual equinox, with fixed, zonally symmetric SST temperatures idealized after the present day climatology. Two year long aqua-planet simulations are performed, using CAM-SE in the *ne30np4*

default configuration, and with the *ne30pg3* physics grid configuration. A plot similar to Figure 3 is constructed for the *ne30pg3* simulation, in which a probability density distribution of upward *omega* in the deep tropics is conditionally sampled based on location within the element. In the *ne30pg3* configuration, the sampling is based on a grid cell index 1-9, corresponding to the control volume location within the element (Figure 3). Through the use of the physics grid, the dynamical state appears independent of location within the element, a marked improvement over the *ne30np4* (Figure 3). Since the state is independent of in-element location, it follows that the physics forcing, which is evaluated from the state, should also be independent of within-element location. The low-level, mean and variance of the physics tendencies in the two aqua-planet simulations are shown in Figure 7. The mean physics tendencies contains modest grid imprinting in the default configuration, while in the variance field, grid imprinting is both ubiquitous and unmistakable (Figure 7). The variance is larger on boundary nodes (Figure 7), resulting in a clear ‘stitching’ pattern resembling the cube-sphere grid. In *ne30pg3*, the grid imprinting is all but eliminated based on the mean and variance of the physics tendencies (Figure 7).

Grid imprinting associated with the flow around obstacles is more problematic than that encountered on the aqua-planets. In order to diagnose grid imprinting associated with topographic flow, an idealized held-suarez configuration (Held and Suarez 1994) is outfitted with real world topography, and ran for a year using the *ne30np4* and *ne30pg3* configurations. Figure 8 shows the mean ω at two different vertical levels in the middle troposphere. At higher latitudes (such as southern Andes), the flow is smooth, conforming reasonably to the underlying topography. At lower latitudes, over the Andes or the Himalayas, there is a clear preference for larger magnitude vertical motion to occur at the element boundaries. The vertical structure of ω in regions of strong grid-imprinting is depicted in Figure 9, which are great-circle distance-pressure transects over the Andes and Himalayas. The ω field indicates large magnitude upward motion occurs as the flow approaches the foot of a topographic obstacle. Compensating downward motion tends to occur about 2 GLL nodes downwind of the strong upward motion (although sometimes they form up-slope). The full troposphere upward-downwawrd couplets are an indication that grid imprinting due to topography is enhanced in regions of weak stratification, such as occurs in the deep tropics, with forced upslope flow facilitating the release of gravitational instability. The greater magnitude vertical motion is a result of the characteristically tighter pressure gradients at element boundaries.

Through the use of the physics grid, grid imprinting due to topographic flow is reduced (Figures 8 and 9). Figures 8 and 9 also show the state in CAM-SE-CSLAM, but on the

dynamical core grid. Arguably, the grid imprinting due to topography in CAM-SE-CSLAM, is not much of an improvement from CAM-SE, from the perspective of the dynamical core grid. The CAM-SE-CSLAM solution does have less grid imprinting, over the Andes and Himalayas, from the perspective of the physics grid. The reduction in grid imprinting is almost entirely a result of the smoothing effect of integrating the basis functions over the control volumes in the physics grid. The native topography lives on the physics grid, and the surface geopotential is mapped to the nodal points at run-time in *ne30pg3*. The mapping method does not introduce new extreme to the nodal points, and the topography tends to be smoother at the element boundaries, relative to *ne30np4*. This effect is rather small, with differences between CAM-SE and CAM-SE-CSLAM topography on the order of a few meters. In regions of gravitational instability, the flow appears damped compared to the *ne30np4* configuration, even from the perspective of the dynamics grid (Figure 9). We speculate that this damped motion may result from the use of a slightly smoother topography, as viewed by the dynamical core grid.

4. Conclusions

Element-based high-order Galerkin Methods possess many of the attractive qualities recommended for next generation global atmospheric models. Among these, high-order accuracy is achieved with minimal communication between elements, allowing for near perfect scaling on massively parallel systems. Element communication amounts to a numerical flux applied to the element boundaries, reconciling overlapping solutions of adjacent elements but degrading the order of accuracy of the boundary nodes in the process (to C^0). For non-smooth problems, gradients are systematically tighter at the element boundaries, and local extrema often characterize the boundary nodes. This behavior is illustrated using NCAR's Community Atmosphere Model with Spectral Elements dynamics (CAM-SE) in an aqua-planet configuration, and in a Held-Suarez configuration with real-world topography.

The authors argue that the conventional physics-dynamics coupling paradigm, in which the physical parameterizations are evaluated on the dynamical core grid, exacerbates grid imprinting by commuting boundary node extrema through the physics forcing. A separate physics grid is proposed and implemented in CAM-SE, and referred to as CAM-SE-CSLAM, through dividing the elements into quasi-equal areas with equivalent degrees of freedom. The state is mapped to the physics grid with high-order accuracy through integrating CAM-SE's Lagrange basis functions over the control volumes. Control volumes near element boundaries now represent a state in the vicinity of the extrema produced through the boundary

exchange operation, as opposed to the the nodal value itself. The physical parameterizations are evaluated on the finite volume grid, and the forcing terms are mapped back to the dynamical core grid **discuss mapping back**. In aqua-planet simulations, evaluating the parameterizations on the physics grid removes any obvious dependence of proximity to the element boundary, resulting in a more realistic state with negligible grid imprinting.

In CAM-SE-CSLAM, the physics grid replaces the finite-volume grid used to compute fluxes between model components in CAM-SE (Figure ??). The appeal here is two-fold. Through integrating the Lagrange basis functions over control volumes, one can be certain that the fluxes computed from this grid are indeed a volume averaged flux. The same can not be said for CAM-SE, where the nodal values are simply assigned to each control volume. The second advantage of the new coupler grid, is that extrema occurring on boundary nodes can no longer commute through other model components, in simulations without topography. In simulations with real world topography, CAM-SE-CSLAM defines the model topography on the physics grid. This provides a modest advantage - mapping topography to the quadrature nodes at run-time ensures that no new extrema will be introduced to the boundary nodes, where the solution is least smooth. This may result in a minor reduction in grid imprinting. A larger reduction in grid imprinting associated with the flow over topography is attributed to the smoothing effect of integrating the basis functions over the control volumes on the physics grid. However, grid imprinting is still observable in CAM-SE-CSLAM, around regions of topography in lower latitudes (and this grid imprinting is passed to the other model components through the coupler grid).

Acknowledgments. NCAR is sponsored by the National Science Foundation (NSF).

References

- Arakawa, A., and W. H. Schubert, 1974: Interaction of a cumulus cloud ensemble with the large-scale environment, Part I. *J. Atmos. Sci.*, **31**, 674–701.
- Bacmeister, J. T., M. F. Wehner, R. B. Neale, A. Gettelman, C. Hannay, P. H. Lauritzen, J. M. Caron, and J. E. Truesdale, 2013: Exploratory high-resolution climate simulations using the community atmosphere model (cam). *J. Climate*, **27** (9), 3073–3099, doi:10.1175/JCLI-D-13-00387.1.
- Brdar, S., M. Baldauf, A. Dedner, and R. Klfkorn, 2013: Comparison of dynamical cores for nwp models: comparison of cosmo and dune. *Theoretical and Computational Fluid Dynamics*, **27** (3-4), 453–472, doi:10.1007/s00162-012-0264-z.
- Dennis, J. M., and Coauthors, 2012: CAM-SE: A scalable spectral element dynamical core for the Community Atmosphere Model. *Int. J. High. Perform. C.*, **26** (1), 74–89, doi:10.1177/1094342011428142, URL <http://hpc.sagepub.com/content/26/1/74.abstract>, <http://hpc.sagepub.com/content/26/1/74.full.pdf+html>.

- Durran, D., 2010: *Numerical Methods for Fluid Dynamics: With Applications to Geophysics*, Texts in Applied Mathematics, Vol. 32. 2nd ed., Springer, 516 p.
- Fournier, A., M. A. Taylor, and J. J. Tribbia, 2004: The spectral element atmosphere model (SEAM): High-resolution parallel computation and localized resolution of regional dynamics. *Mon. Wea. Rev.*, **132** (3), 726–748.
- Giraldo, F., and M. Restelli, 2008: A study of spectral element and discontinuous galerkin methods for the Navier-Stokes equations in nonhydrostatic mesoscale atmospheric modeling: Equation sets and test cases. *J. Comput. Phys.*, **227** (8), 3849 – 3877, doi:<http://dx.doi.org/10.1016/j.jcp.2007.12.009>.
- Guba, O., M. A. Taylor, P. A. Ullrich, J. R. Overfelt, and M. N. Levy, 2014: The spectral element method (sem) on variable-resolution grids: evaluating grid sensitivity and resolution-aware numerical viscosity. *Geosci. Model Dev.*, **7** (6), 2803–2816, doi:[10.5194/gmd-7-2803-2014](https://doi.org/10.5194/gmd-7-2803-2014).
- Held, I. M., and M. J. Suarez, 1994: A proposal for the intercomparison of the dynamical cores of atmospheric general circulation models. *Bull. Am. Meteorol. Soc.*, **73**, 1825–1830.
- Kim, Y.-J., F. X. Giraldo, M. Flatau, C.-S. Liou, and M. S. Peng, 2008: A sensitivity study of the kelvin wave and the Madden-Julian oscillation in aquaplanet simulations by the Naval Research Laboratory Spectral Element Atmospheric Model. *J. Geo. Res.: Atmospheres*, **113** (D20), doi:[10.1029/2008JD009887](https://doi.org/10.1029/2008JD009887), d20102.
- Lauritzen, P. H., and Coauthors, 2017: Ncar cesm2.0 release of camse: A reformulation of the spectral-element dynamical core in dry-mass vertical coordinates with comprehensive treatment of condensates and energy. *J. Adv. Model. Earth Syst.*, in prep.
- Medeiros, B., D. L. Williamson, and J. G. Olson, 2016: Reference aquaplanet climate in the community atmosphere model, version 5. *J. Adv. Model. Earth Syst.*, **8** (1), 406–424, doi:[10.1002/2015MS000593](https://doi.org/10.1002/2015MS000593).
- Nair, R., H.-W. Choi, and H. Tufo, 2009: Computational aspects of a scalable high-order discontinuous galerkin atmospheric dynamical core. *Computers & Fluids*, **38** (2), 309 – 319, doi:<http://dx.doi.org/10.1016/j.compfluid.2008.04.006>.
- Nair, R. D., M. N. Levy, and P. H. Lauritzen, 2011: Emerging numerical methods for atmospheric modeling, in: P.H. Lauritzen, R.D. Nair, C. Jablonowski, M. Taylor (Eds.), Numerical techniques for global atmospheric models. *Lecture Notes in Computational Science and Engineering*, Springer, **80**.
- Neale, R. B., and B. J. Hoskins, 2000: A standard test for agcm's including their physical parametrizations: I: the proposal. *Atmos. Sci. Lett.*, **1** (2), 101–107, doi:[10.1006/asle.2000.0022](https://doi.org/10.1006/asle.2000.0022).
- Neale, R. B., and Coauthors, 2010: Description of the NCAR Community Atmosphere Model (CAM 5.0). NCAR Technical Note, National Center of Atmospheric Research.
- Plant, G. C. C., R. S., 2008: A stochastic parameterization for deep convection based on equilibrium statistics. *J. Atmos. Sci.*, **65**, 87–105, doi:[10.1175/2007JAS2263.1](https://doi.org/10.1175/2007JAS2263.1), URL <http://dx.doi.org/10.1175/2007JAS2263.1>.
- Reed, K. A., J. T. Bacmeister, N. A. Rosenbloom, M. F. Wehner, S. C. Bates, P. H. Lauritzen, J. E. Truesdale, and C. Hannay, 2015: Impact of the dynamical core on the direct simulation of tropical cyclones in a high-resolution global model. *Geophys. Res. Lett.*, **42** (9), 3603–3608, doi:[10.1002/2015GL063974](https://doi.org/10.1002/2015GL063974).
- Rhoades, A. M., X. Huang, P. A. Ullrich, and C. M. Zarzycki, 2016: Characterizing sierra nevada snowpack using variable resolution cesm. *J. Appl. Meteor. Climatol.*, **55**, doi:[10.1175/JAMC-D-15-0156.1](https://doi.org/10.1175/JAMC-D-15-0156.1), URL <http://dx.doi.org/10.1175/JAMC-D-15-0156.1>.
- Small, R. J., and Coauthors, 2014: A new synoptic scale resolving global climate simulation using the community earth system model. *Journal of Advances in Modeling Earth Systems*, **6** (4), 1065–1094, doi:[10.1002/2014MS000363](https://doi.org/10.1002/2014MS000363).
- Taylor, M., J. Edwards, and A. St-Cyr, 2008: Petascale atmospheric models for the community climate system model: new developments and evaluation of scalable dynamical cores. *J. Phys.: Conf. Ser.*, **125**, doi:[10.1088/1742-6596/125/1/012023](https://doi.org/10.1088/1742-6596/125/1/012023).
- Taylor, M. A., and A. Fournier, 2010: A compatible and conservative spectral element method on unstructured grids. *J. Comput. Phys.*, **229** (17), 5879 – 5895, doi:[10.1016/j.jcp.2010.04.008](https://doi.org/10.1016/j.jcp.2010.04.008).
- Ullrich, P. A., and M. A. Taylor, 2015: Arbitrary-order conservative and consistent remapping and a theory of linear maps: Part I. *Mon. Wea. Rev.*, **143**, 2419–2440, doi:[10.1175/MWR-D-14-00343.1](https://doi.org/10.1175/MWR-D-14-00343.1).
- Zarzycki, C. M., C. Jablonowski, and M. A. Taylor, 2014a: Using variable-resolution meshes to model tropical cyclones in the community atmosphere model. *Mon. Wea. Rev.*, **142** (3), 1221–1239, doi:[10.1175/MWR-D-13-00179.1](https://doi.org/10.1175/MWR-D-13-00179.1).
- Zarzycki, C. M., M. N. Levy, C. Jablonowski, J. R. Overfelt, M. A. Taylor, and P. A. Ullrich, 2014b: Aquaplanet experiments using cam's variable-resolution dynamical core. *J. Climate*, **27** (14), 5481–5503, doi:[10.1175/JCLI-D-14-00004.1](https://doi.org/10.1175/JCLI-D-14-00004.1).

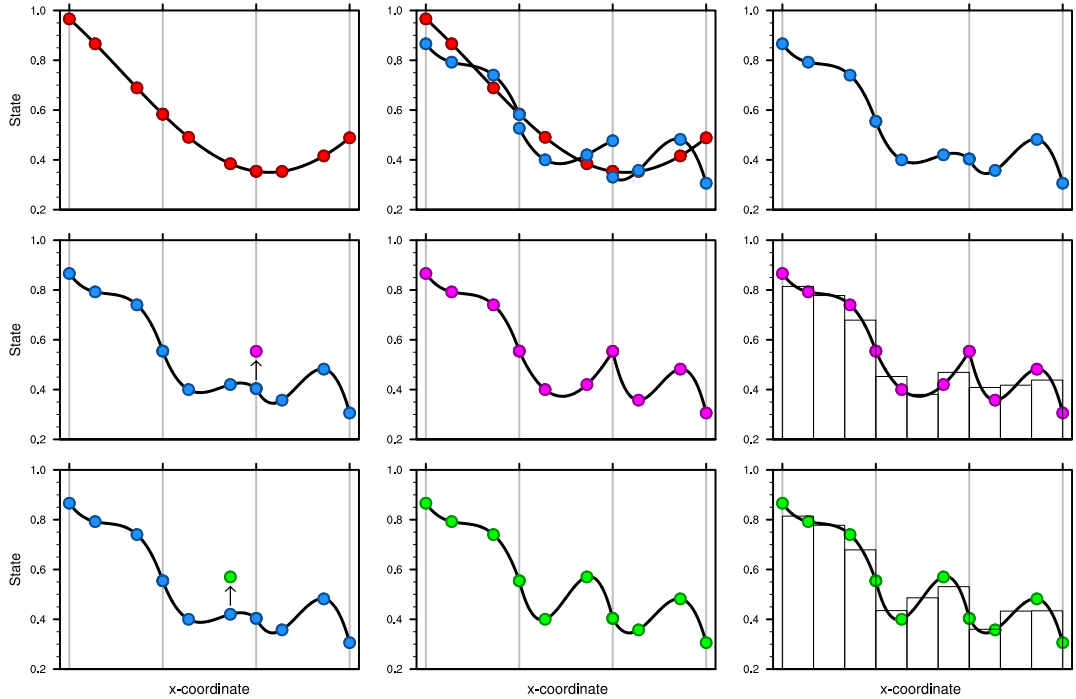


FIG. 4. A 1D schematic illustration on how CAM-SE advances the solution to the equations of motion in time. Consider 3 elements. The red filled circles are the GLL quadrature points in each element ($np = 4$). Note that the quadrature points on the boundary are shared between elements. (a) Assume a degree 3 global Lagrange polynomial initial condition (red curve) which can be represented exactly by the degree 3 Lagrange basis in each element. (b) The solution to the equations of motion are advanced in time (one Runga-Kutta step) independently in each element leading to the quadrature values marked with filled purple circles. The Lagrange basis is shown with red curves connecting the purple circles. There are now two solutions, one from left and one from right, for the quadrature points at the element end points. In CAM-SE the values are averaged so that the solution is C^0 . Note that the averaging changes the Lagrange polynomials throughout except at the internal quadrature points. (c) shows the solution after averaging. (d) Assume there is a grid-scale forcing that increases the quadrature value located at $x = 3$. (e) The solution is now clearly C^0 at the element boundary at $x = 3$. (f) Histograms shows the average values resulting in integrating the basis functions over the control

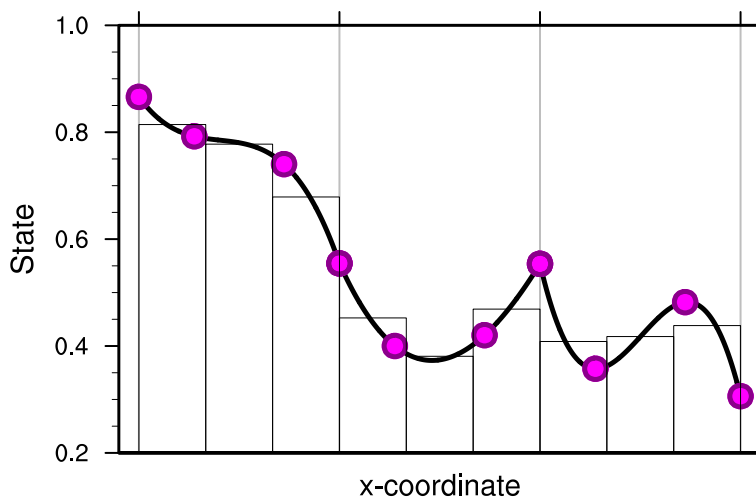


FIG. 5. A graphical illustration of the physics grid in one dimension. Three elements are shown and the filled red circles are the GLL quadrature points in each element. The red curve is the basis function representation of the field and the green filled circles are the quadrature point values. The physics grid divides each element into 3 equal-area control volumes. The histogram shows the average values over the physics grid control volumes resulting from integrating the basis functions over the respective control volumes.

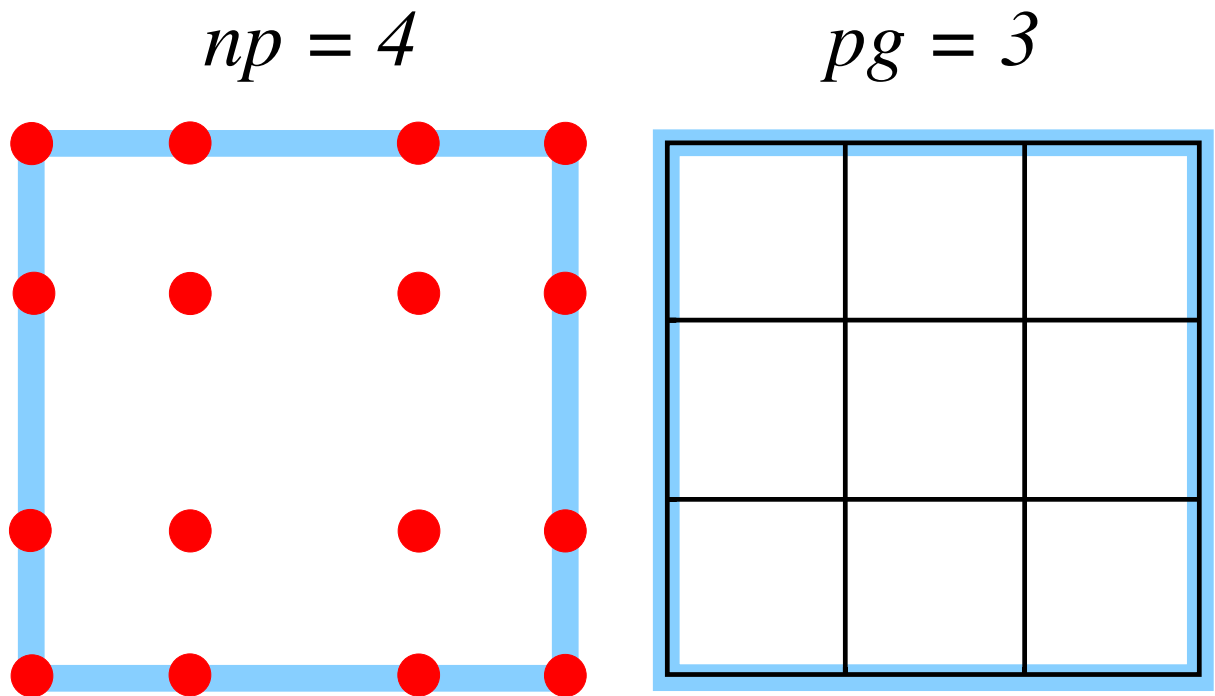


FIG. 6. A schematic illustration of an element, indicating the relationship between (left) the dynamical core grid, and (right) the proposed quasi-equal area physics grid. The physics grid contains $pg \times pg$ grid cells in each element, and $pg = 3$.

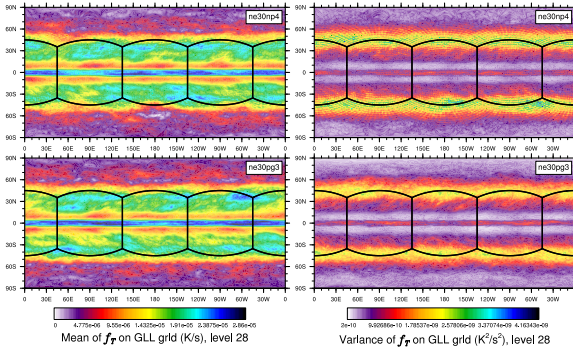


FIG. 7. Mean (left) and variance (right) of the low level temperature tendencies from the physical parameterizations on the GLL grid, with the *ne30np4* configuration, top row) and *ne30pg3* configuration (bottom row), in a pair of year-long aqua-planet simulations after Medeiros et al. (2016). Grid imprinting is observed along the element boundaries in *ne30np4*, but is absent from the *ne30pg3* simulation.

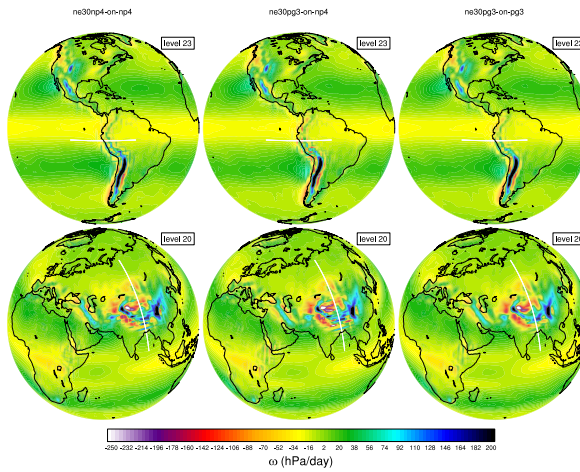


FIG. 8. Mean ω at two model levels in the middle troposphere, in a Held-Suarez configuration outfitted with real world topography. (Left) CAM-SE state on the GLL grid, *ne30np4*, (Middle) CAM-SE-CSLAM state on the GLL grid, *ne30np4* and (Right) CAM-SE-CSLAM state on the physics grid, *ne30pg3*. The ω fields are computed from a 1200 day Held-Suarez simulation. White lines denote the great circle transects in 9.

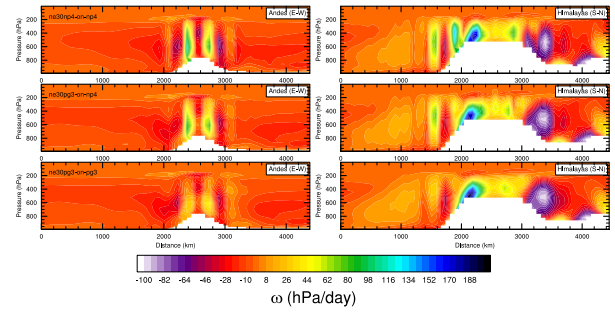


FIG. 9. Great circle distance-pressure transect of ω in the Held-Suarez simulations with realistic topography. ω field derived from the final 12 months of a 13 month simulation.